EUROPEAN ORGANISATION FOR NUCLEAR RESEARCH

CERN-PPE/90-121
22 August 1990

A Measurement of Energy Correlations and a Determination of $\alpha_s(M^2_{Z^0})$ in e^+e^- Annihilations at $\sqrt{s} = 91$ GeV

The OPAL Collaboration

Abstract

From an analysis of multi-hadron events from Z^0 decays, values of the strong coupling constant $\alpha_s(M^2_{Z^0}) = 0.131 \pm 0.006\,(\text{exp.}) \pm 0.007\,(\text{theor.})$ and $\alpha_s(M^2_{Z^0}) = 0.117^{+0.007}_{-0.009}\,(\text{exp.})\,^{+0.006}_{-0.002}$ (theor.) are derived from the energy-energy correlation distribution and its asymmetry, respectively, assuming the QCD renormalization scale $\mu = M_{Z^0}$. The theoretical error accounts for differences between $O(\alpha_s^2)$ calculations. A two parameter fit of $\Lambda_{\overline{MS}}$ and the renormalization scale μ leads to $\Lambda_{\overline{MS}} = 216 \pm 85$ MeV and $(\mu^2/s) = 0.027 \pm 0.013$ or to $\alpha_s(M^2_{Z^0}) = 0.117^{+0.006}_{-0.008}\,(\text{exp.})$ for the energy-energy correlation distribution. The energy-energy correlation asymmetry distribution is insensitive to a scale change: thus the α_s value quoted above for this variable includes the theoretical uncertainty associated with the renormalization scale.

(Submitted to Physics Letters B)

The OPAL Collaboration

M.Z. Akrawy[11], G. Alexander[21], J. Allison[14], P.P. Allport[5], K.J. Anderson[8], J.C. Armitage[6], G.T.J. Arnison[18], P. Ashton[14], G. Azuelos[16,f], J.T.M. Baines[14], A.H. Ball[15], J. Banks[14], G.J. Barker[11], R.J. Barlow[14], J.R. Batley[5], A. Beck[21], J. Becker[9], T. Behnke[7], K.W. Bell[18], G. Bella[21], S. Bethke[10], O. Biebel[3], U. Binder[9], I.J. Bloodworth[1], P. Bock[10], H. Breuker[7], R.M. Brown[18], R. Brun[7], A. Buijs[7], H.J. Burckhart[7], P. Capiluppi[2], R.K. Carnegie[6], A.A. Carter[11], J.R. Carter[5], C.Y. Chang[15], D.G. Charlton[7], J.T.M. Chrin[14], P.E.L. Clarke[23], I. Cohen[21], W.J. Collins[5], J.E. Conboy[13], M. Couch[1], M. Coupland[12], M. Cuffiani[2], S. Dado[20], G.M. Dallavalle[2], P. Debu[19], M.M. Deninno[2], A. Dieckmann[10], M. Dittmar[4], M.S. Dixit[17], E. Duchovni[24], I.P. Duerdoth[7,d], D.J.P. Dumas[6], H. El Mamouni[16], P.A. Elcombe[5], P.G. Estabrooks[6], E. Etzion[21], F. Fabbri[2], P. Farthouat[19], H.M. Fischer[3], D.G. Fong[15], M.T. French[18], C. Fukunaga[22], A. Gaidot[19], O. Ganel[24], J.W. Gary[10], J. Gascon[16], N.I. Geddes[18], C.N.P. Gee[18], C. Geich-Gimbel[3], S.W. Gensler[8], F.X. Gentit[19], G. Giacomelli[2], V. Gibson[5], W.R. Gibson[11], J.D. Gillies[18], J. Goldberg[20], M.J. Goodrick[5], W. Gorn[4], D. Granite[20], E. Gross[24], J. Grunhaus[21], H. Hagedorn[9], J. Hagemann[7], M. Hansroul[7], C.K. Hargrove[17], I. Harrus[20], J. Hart[5], P.M. Hattersley[1], M. Hauschild[7], C.M. Hawkes[7], E. Heflin[4], R.J. Hemingway[6], R.D. Heuer[7], J.C. Hill[5], S.J. Hillier[1], C. Ho[4], J.D. Hobbs[8], P.R. Hobson[23], D. Hochman[24], B. Holl[7], R.J. Homer[1], S.R. Hou[15], C.P. Howarth[13], R.E. Hughes-Jones[14], R. Humbert[9], P. Igo-Kemenes[10], H. Ihssen[10], D.C. Imrie[23], L. Janissen[6], A. Jawahery[15], P.W. Jeffreys[18], H. Jeremie[16], M. Jimack[7], M. Jobes[1], R.W.L. Jones[11], P. Jovanovic[1], D. Karlen[6], K. Kawagoe[22], T. Kawamoto[22], R.G. Kellogg[15], B.W. Kennedy[13], C. Kleinwort[7], D.E. Klem[17], G. Knop[3], T. Kobayashi[22], T.P. Kokott[3], L. Köpke[7], R. Kowalewski[6], H. Kreutzmann[3], J. Kroll[8], M. Kuwano[22], P. Kyberd[11], G.D. Lafferty[14], F. Lamarche[16], W.J. Larson[4], J.G. Layter[4], P. Le Du[19], P. Leblanc[16], A.M. Lee[15], M.H. Lehto[13], D. Lellouch[7], P. Lennert[10], L. Lessard[16], L. Levinson[24], S.L. Lloyd[11], F.K. Loebinger[14], J.M. Lorah[15], B. Lorazo[16], M.J. Losty[17], J. Ludwig[9], J. Ma[4,b], A.A. Macbeth[14], M. Mannelli[7], S. Marcellini[2], G. Maringer[3], A.J. Martin[11], J.P. Martin[16], T. Mashimo[22], P. Mättig[7], U. Maur[3], T.J. McMahon[1], J.R. McNutt[23], F. Meijers[7], D. Menszner[10], F.S. Merritt[8], H. Mes[17], A. Michelini[7], R.P. Middleton[18], G. Mikenberg[24], J. Mildenberger[6], D.J. Miller[13], C. Milstene[21], M. Minowa[22], W. Mohr[9], A. Montanari[2], T. Mori[22], M.W. Moss[14], P.G. Murphy[14], W.J. Murray[5], B. Nellen[3], H.H. Nguyen[8], M. Nozaki[22], A.J.P. O'Dowd[14], S.W. O'Neale[7,c], B.P. O'Neill[4], F.G. Oakham[17], F. Odorici[2], M. Ogg[6], H. Oh[4], M.J. Oreglia[8], S. Orito[22], J.P. Pansart[19], G.N. Patrick[18], S.J. Pawley[14], P. Pfister[9], J.E. Pilcher[8], J.L. Pinfold[21], D.E. Plane[7], B. Poli[2], A. Pouladdej[6], E. Prebys[7], T.W. Pritchard[11], G. Quast[7], J. Raab[7], M.W. Redmond[8], D.L. Rees[1], M. Regimbald[16], K. Riles[4], C.M. Roach[5], S.A. Robins[11], A. Rollnik[3], J.M. Roney[8], S. Rossberg[9], A.M. Rossi[2,a], P. Routenburg[6], K. Runge[9], O. Runolfsson[7], S. Sanghera[6], R.A. Sansum[18], M. Sasaki[22], B.J. Saunders[18], A.D. Schaile[9], O. Schaile[9], W. Schappert[6], P. Scharff-Hansen[7], S. Schreiber[3], J. Schwarz[9], A. Shapira[24], B.C. Shen[4], P. Sherwood[13], A. Simon[3], P. Singh[11], G.P. Siroli[2], A. Skuja[15], A.M. Smith[7], T.J. Smith[1], G.A. Snow[15], R.W. Springer[15], M. Sproston[18], K. Stephens[14], H.E. Stier[9], R. Strohmer[10], D. Strom[8], H. Takeda[22], T. Takeshita[22], N.J. Thackray[1], T. Tsukamoto[22], M.F. Turner[5], G. Tysarczyk-Niemeyer[10], D. Van den plas[16], G.J. VanDalen[1], G. Vasseur[19], C.J. Virtue[17], H. von der Schmitt[10], J. von Krogh[10], A. Wagner[10], C. Wahl[9], J.P. Walker[1], C.P. Ward[5], D.R. Ward[5], P.M. Watkins[1], A.T. Watson[1], N.K. Watson[1], M. Weber[10], S. Weisz[7], P.S. Wells[7], N. Wermes[10], M. Weymann[7], G.W. Wilson[19], J.A. Wilson[1], I. Wingerter[7], V-H. Winterer[9], N.C. Wood[13], S. Wotton[7], B. Wuensch[3], T.R. Wyatt[14], R. Yaari[24], Y. Yang[4,b], G. Yekutieli[24], T. Yoshida[22], W. Zeuner[7], G.T. Zorn[15].

[1]School of Physics and Space Research, University of Birmingham, Birmingham, B15 2TT, UK
[2]Dipartimento di Fisica dell' Università di Bologna and INFN, Bologna, 40126, Italy
[3]Physikalisches Institut, Universität Bonn, D-5300 Bonn 1, FRG
[4]Department of Physics, University of California, Riverside, CA 92521 USA
[5]Cavendish Laboratory, Cambridge, CB3 0HE, UK
[6]Carleton University, Dept of Physics, Colonel By Drive, Ottawa, Ontario K1S 5B6, Canada
[7]CERN, European Organisation for Particle Physics, 1211 Geneva 23, Switzerland
[8]Enrico Fermi Institute and Department of Physics, University of Chicago, Chicago Illinois 60637, USA
[9]Fakultät für Physik, Albert Ludwigs Universität, D-7800 Freiburg, FRG
[10]Physikalisches Institut, Universität Heidelberg, Heidelberg, FRG
[11]Queen Mary and Westfield College, University of London, London, E1 4NS, UK
[12]Birkbeck College, London, WC1E 7HV, UK
[13]University College London, London, WC1E 6BT, UK
[14]Department of Physics, Schuster Laboratory, The University, Manchester, M13 9PL, UK
[15]Department of Physics and Astronomy, University of Maryland, College Park, Maryland 20742, USA
[16]Laboratoire de Physique Nucléaire, Université de Montréal, Montréal, Quebec, H3C 3J7, Canada
[17]National Research Council of Canada, Herzberg Institute of Astrophysics, Ottawa, Ontario K1A 0R6, Canada
[18]Rutherford Appleton Laboratory, Chilton, Didcot, Oxfordshire, OX11 0QX, UK
[19]DPhPE, CEN Saclay, F-91191 Gif-sur-Yvette, France
[20]Department of Physics, Technion-Israel Institute of Technology, Haifa 32000, Israel
[21]Department of Physics and Astronomy, Tel Aviv University, Tel Aviv 69978, Israel
[22]International Centre for Elementary Particle Physics and Dept of Physics, University of Tokyo, Tokyo 113, and Kobe University, Kobe 657, Japan
[23]Brunel University, Uxbridge, Middlesex, UB8 3PH UK
[24]Nuclear Physics Department, Weizmann Institute of Science, Rehovot, 76100, Israel

[a]Present address: Dipartimento di Fisica, Università della Calabria and INFN, 87036 Rende, Italy
[b]On leave from Harbin Institute of Technology, Harbin, China
[c]Now at Applied Silicon Inc
[d]On leave from Manchester University
[e]On leave from Birmingham University
[f]and TRIUMF, Vancouver, Canada

1 Introduction

Energy-energy correlations (EEC) of hadronic events were first introduced by Basham *et al.* [1] as an experimental observable sensitive to the value of the coupling constant α_s of Quantum Chromodynamics (QCD). They are defined, in practice, as the histogram of the angle between all combinations of pairs of particles in hadronic events, weighted by their normalized energies, and averaged over all events:

$$EEC(\chi) = \frac{2}{\Delta\chi \cdot N} \int_{\chi-\frac{\Delta\chi}{2}}^{\chi+\frac{\Delta\chi}{2}} \sum_{events}^{N} \sum_{i,j} \frac{E_i E_j}{E_{vis}^2} \delta(\chi' - \chi_{ij}) d\chi', \tag{1}$$

where χ_{ij} is the angle between particles i and j and $\Delta\chi$ is the width of the histogram bin. Two-jet events yield a distribution sharply peaked near $\chi = 0^0$ and $\chi = 180^0$, whereas events with hard gluon radiation fill the central region in a non-symmetric fashion. The shape of the distribution is therefore correlated with the value of α_s. The energy-energy correlation asymmetry (AEEC)

$$AEEC(\chi) = EEC(\pi - \chi) - EEC(\chi) \tag{2}$$

removes the two-jet component and so is particularly sensitive to α_s. AEEC has a smaller 2nd order QCD correction than EEC and is subject to smaller theoretical and experimental errors because of the cancelations implicit in (2).

Analytic formulae for EEC and AEEC to $O(\alpha_s^2)$ perturbation theory have been presented by several groups, to be referred to here as AB [2], RSE [3], FK [4] and KN [5]. Monte Carlo calculations also provide predictions for the energy correlation distributions. The $O(\alpha_s^2)$ matrix element formulae of ERT [6] and GKS [7] are incorporated into the Jetset Monte Carlo [8] and provide a convenient means for this.

In this letter we present measurements of energy correlations in hadronic Z^0 decays, by the OPAL Collaboration. From the energy weighted cross sections, values of α_s are extracted for both analytic and Monte Carlo calculations. The coupling constant $\alpha_s(\mu^2)$ can be written as a function of $ln(\mu^2/\Lambda^2_{\overline{MS}})$, where μ is the QCD renormalization scale. In a first step, we adjust $\Lambda_{\overline{MS}}$ through comparison with the measured EEC and AEEC distributions, assuming $\mu^2 = M^2_{Z^0}$. In a second step, $\Lambda_{\overline{MS}}$ and μ are adjusted together, in a 2 parameter fit. This study complements our previous evaluation of $\Lambda_{\overline{MS}}$ and μ at the Z^0 peak, using the jet rates [9]. Unlike the jet rates, energy correlations do not rely on a jet resolution parameter or an event-by-event analysis. Values of α_s extracted from EEC and AEEC distributions at lower c.m. energies in e^+e^- annihilations have been reported in [10]-[21]. It is expected that second-order perturbative calculations yield more reliable results at Z^0 energies than at lower energies, because the value of the coupling constant is smaller. Furthermore, hadronization corrections are smaller for the higher energy, reducing the uncertainty in the comparison of calculations with data.

2 Data Selection

The data were recorded with the OPAL detector [22] at the CERN e^+e^- collider LEP. The tracking of charged particles is performed with the central tracking detector, composed of a vertex chamber, a jet chamber and a chamber for measurements in the r-θ direction, all enclosed by a solenoidal magnet coil (r is the coordinate normal to the beam axis; θ is the polar angle). The principal tracking detector is the jet chamber, which provides up to 159 space-points and close to 100% track finding efficiency for charged tracks in the region $|cos\theta| < 0.92$. For the present analysis, the average angular resolution is particularly relevant: for charged tracks this is about 20 mrad in the r-θ direction and better than 1 mrad in the direction perpendicular to the beam axis. Electromagnetic energy deposits ("clusters") are measured with the electromagnetic calorimeter, a detector of lead-glass blocks located in both the barrel and endcap regions, each block of 40x40 mrad^2 cross section, for a total detector solid angle coverage of 98% of 4π.

The trigger and online event selection for hadronic events are described in [23]. We applied additional criteria for this analysis to reduce the small level of background and to obtain well contained events. Charged tracks were accepted if they originated from within 5 cm of the interaction point in the direction perpendicular to the beam axis. The minimum transverse momentum was set at 150 MeV, the angle to the beam direction had to exceed 20 degrees and the track was required to have at least 40 measured space-points. Electromagnetic clusters were accepted if they had at least 100 or 150 MeV of energy, depending on whether they appeared in the barrel or endcap. Hadronic events were required to contain at least 5 charged tracks and a polar angle for the thrust direction, defined using the accepted charged tracks and electromagnetic clusters, in the range $|cos(\theta_{thrust})| < 0.87$. From the data sample of 3.6 pb^{-1} used for this analysis, we obtained 69,991 events at $\sqrt{s} = 88.3$ -- 95.0 GeV after all cuts.

3 Energy Correlation Measurements

In figure 1 and in table 1 are presented the measured EEC and AEEC distributions at 91 GeV, unfolded for detector acceptance and resolution and for initial-state photon radiation. The bin widths of 3.6° are well within the limits of the experimental angular resolution. The unfolding procedure is based on a detailed simulation of the OPAL detector and is described in [24]. It leads to bin-by-bin correction constants defined, for EEC, by

$$(EEC^{data}_{hadron})_i = \left[\frac{(EEC^{M.C.}_{gen.})_i}{(EEC^{M.C.}_{det.})_i}\right] \cdot (EEC^{data}_{meas.})_i \quad ; \quad i = \text{bin index}, \tag{3}$$

where "gen." refers to Monte Carlo events at the generator level, without initial-state radiation or detector simulation and including charged and neutral particles with lifetimes greater than $3{\cdot}10^{-10}$s, while "det." refers to Monte Carlo events with initial-state radiation and detector simulation, which have been passed through the same reconstruction and selection algorithms as the data. $EEC^{data}_{meas.}$ and EEC^{data}_{hadron} are the measured and unfolded distributions, respectively. For the measurements we use both charged tracks and electromagnetic

clusters, with no correction for the overlap of energy deposited by charged and neutral particles. The unfolded AEEC is derived from the unfolded EEC. The correction constants are defined by the terms in square brackets in (3); to obtain these constants we use the Jetset parton shower model [8] with parameter values adjusted to describe global event shapes measured by OPAL [24]. This model plus detector simulation provides a good description of the energy correlation measurements before the corrections are applied, making it suitable for the calculation of these constants. The values of the corrections, shown in the inset above figure 1 (a), vary between about 0.90 and 1.20.

The statistical errors of the EEC and AEEC distributions have strong bin-to-bin correlations. To evaluate these errors, we generated 10 different samples of Monte Carlo events, each with the same statistics as the data sample. The statistical error was set equal to the RMS deviation which was observed, for each bin. The systematic error from the correction procedure was measured as follows. Monte Carlo events including detector simulation and initial-state radiation were generated using the Herwig shower model [25], to form a mock "data" sample. The default parameter values of Herwig, which essentially arise from measurements by our experiment [24], were used. The Herwig description of the measured distributions is reasonably good at this level. The EEC distribution from these Herwig events was unfolded using the same Jetset correction values which are applied to the data. The difference between the unfolded Herwig "data" distribution and the Herwig distribution constructed at the generator level was taken as the systematic error introduced by the correction procedure, bin-by-bin. Additional systematic errors due to imperfections in the simulation of the detector or in the event reconstruction were estimated by taking the difference between the unfolded distributions derived from the tracking chambers alone to those derived from the calorimeter alone. We also tested the sensitivity of the correction factors to the z resolution of the jet chamber, by varying the simulated resolution for the z hit position between 6 and 20 cm, and found the error due to this source to be negligible. The different systematic errors were added in quadrature to define the total systematic error. Also shown in figure 1 are the generator level predictions of Jetset and Herwig. Jetset provides a good decription of the unfolded measurements, while the prediction of Herwig is low in the central angular region. In addition, the shape of AEEC from Herwig deviates somewhat from the data.

At $\sqrt{s}=M_{Z^0}$, corrections due to confinement (fragmentation) are in general small, permitting the experimental measurements to be unfolded to the parton level. That QCD parton shower models with different mechanisms for fragmentation describe the detailed features of hadronic event structure from $\sqrt{s} = 30$ to 91 GeV using energy independent parameters [24], implies that the size of these corrections may be estimated reliably. In figure 2 (a) and (b) are shown the measured EEC and AEEC distributions unfolded to the parton level using Jetset and Herwig with the parameter values discussed above. The unfolding is performed according to

$$(EEC^{data}_{parton})_i = \left[\frac{(EEC^{M.C.}_{parton})_i}{(EEC^{M.C.}_{det.})_i}\right] \cdot (EEC^{data}_{meas.})_i \quad ; \quad i = \text{ bin index} \tag{4}$$

in analogy with (3), where EEC^{data}_{parton} is the experimental distribution at the parton level. The unfolded AEEC is obtained from the unfolded EEC, as before. Both the Jetset and Herwig corrections are derived using the default values for the scale Q_0 at which shower development

is halted: $Q_0 = 1$ GeV for Jetset and $Q_0 = 0.65$ GeV for Herwig (the quark masses are left at their default values). Also shown in figure 2 as the solid lines are the hadron level measured distributions, repeated from figure 1. In the angular intervals used to determine α_s, 43.2-136.8° for EEC and 28.8-90.0° for AEEC, the overall corrections, from the level including detector effects to the parton level, have an approximately constant value of about 0.85 for EEC, leading to an effective correction between about 0.8 and 1.2 for AEEC. The effective correction for AEEC is defined as the ratio between the detector and parton level distributions for that quantity. We do not rescale the EEC distribution so that its integral from 0° to 180° is unity, after the corrections to the parton level have been applied, because this procedure relies, in part, on the unfolded distribution at $\chi \approx 0°$ and $\chi \approx 180°$ where the corrections are large (see figure 2). We find that the integral of EEC over its entire range deviates from unity by 2%, after the corrections. This effect is included as a systematic uncertainty in the overall normalization as discussed below. In figure 2 the errors are statistical only and are derived for each bin in the same way as for the hadron level distributions of figure 1.

4 Determination of $\alpha_s(M^2_{Z^0})$

Our analysis for α_s is performed by comparing the parton level corrected measurements to $O(\alpha_s^2)$ theoretical calculations. The corrections are derived from parton shower models. Therefore the goodness of the description of the unfolded measurements by the theory is a test of its adequacy at the Z^0 peak and of the importance of missing higher order terms. According to the suggestions of Kunszt and Nason, this strategy provides a clean test of $O(\alpha_s^2)$ QCD because of the clear separation of the perturbative and fragmentation components [5]. In contrast, it has been common at lower energies to extract α_s from energy correlation measurements through parameter adjustment of an $O(\alpha_s^2)$ Monte Carlo with fragmentation model to describe hadron level distributions. In this case the perturbative and fragmentation components are not well separated and the latter can hide deficiencies of the former. This problem becomes more acute for the higher energy of LEP because of the largeness of the minimum invariant mass value between parton pairs (the value $\sqrt{0.01 \cdot s}$, which is the minimum mass value between parton pairs for $O(\alpha_s^2)$ Monte Carlo generators, as discussed below, is about 9 GeV for $\sqrt{s} = 91$ GeV). Thus we do not employ this method.

Calculations of EEC to $O(\alpha_s^2)$ consist of replacing the event average in (1) by the square of the matrix element for 2-, 3- and 4-parton final states and integrating over the allowed phase space. For the analytic calculations, the EEC distribution can be expressed as

$$EEC(\chi) = \frac{\alpha_s(Q^2)}{\pi} \cdot A(\chi) \; + \; \left(\frac{\alpha_s(Q^2)}{\pi}\right)^2 \cdot B(\chi) \qquad (5)$$

and analogously for AEEC. The 1st order term $A(\chi)$ describes $q\bar{q}$ and $q\bar{q}g$ final states while the 2nd order term $B(\chi)$ describes $q\bar{q}gg$ and $q\bar{q}q'\bar{q}'$ states as well as corrections to $q\bar{q}$ and $q\bar{q}g$. The cross section for each n-parton final state is infrared and collinear divergent. The divergences cancel in the sum over all event types [26]. Different groups have used different methods to cancel singularities in the 2nd order term $B(\chi)$. The results of KN agree better with those of AB than with those of RSE or FK: the disagreements are not well understood [5]. For Monte

Carlo calculations, it is necessary to remove the singularities individually for the 2-, 3- and 4-parton components. This is done by introducing jet resolution criteria by which parton pairs which fail the criteria are combined into a single "jet." The GKS and ERT matrix element Monte Carlos in Jetset employ y_{min} as the resolution parameter, where $\sqrt{y_{min} \cdot s}$ is the minimum invariant mass value allowed between parton pairs. For the Monte Carlo event generation, we use the value y_{min}=0.01, which is essentially the smallest which is possible if the n-parton cross sections are to remain positive in all regions of phase space [27]. Analytic calculations of EEC and AEEC do not require jet resolution criteria, but they are sometimes introduced nonetheless. The FK analytic formula [4] use the jet resolution parameter y_{min}. For these analytic formula, an arbitrarily small value of y_{min} may be used, permitting the effect of the restriction y_{min} = 0.01 for the Monte Carlo calculations to be studied.

The y_{min} cut has an important effect on the shape and height of the Monte Carlo predictions, even for the region of hard gluon radiation. The integral of the 1st order term $A(\chi)$, between 45-135° for EEC and 30-90° for AEEC, is changed by +10.5% and -2.8%, respectively, if y_{min} changes from 0.01 to 0.0001. The corresponding change for the 2nd order term $B(\chi)$ is +30% for EEC and -18% for AEEC [4]. A reduction of y_{min} from 0.01 to 0.0001 reduces the minimum invariant mass value between partons from about 9 GeV to about 1 GeV for $\sqrt{s} = 91$ GeV. Thus y_{min}=0.0001 corresponds well to the scale of virtuality $Q_0 \approx 1$ GeV of the corrected data, making it an appropriate choice for our analysis. We therefore correct the Monte Carlo predictions (ERT and GKS), for the EEC and AEEC measurements in the intervals used to extract α_s, by the ratio of the corresponding values for y_{min}=0.0001 to that for y_{min}=0.01, which are obtained from the FK formulae. This correction is evaluated for each $\Lambda_{\overline{MS}}$ value for which ERT and GKS samples are generated, and has an overall value of about 1.15 for EEC and 0.94 for AEEC.

In figure 3 (a) and (b) the integrated values of the parton level unfolded measurements are presented, along with the theoretical predictions. The range of integration is 43.2-136.8° for EEC and 28.8-90.0° for AEEC. The data are shown for 4 conditions: (i) unfolded with Jetset corrections, (ii) unfolded with Herwig corrections, and unfolded with Jetset corrections but using (iii) charged track information only or (iv) calorimeter information only for the factors $EEC^{data}_{meas.}$ and $EEC^{M.C.}_{det.}$ in (4). The statistical errors of the measurements, derived as explained in section 3, are shown by the bands on the data values. The theoretical predictions are displayed for different values of $\Lambda_{\overline{MS}}$, using the 2-loop β-function as given in [28] with 5 active quark flavors, to relate α_s and $\Lambda_{\overline{MS}}$. The renormalization scale $\mu = M_{Z^0}$ is assumed in all cases. The GKS and ERT predictions have been corrected to y_{min} = 0.0001 as explained above. Figure 3 (a) puts into evidence the differences between the AB, KN and RSE calculations, as reported in [5]. As well, a clear difference appears between GKS and ERT, as has been discussed previously [20,21].

In table 2 the values of $\Lambda_{\overline{MS}}$ and $\alpha_s(M^2_{Z^0})$ which are extracted from comparison to the measurements are presented, for each theoretical calculation separately. For the analytic formulae, AB, RSE, KN and FK, χ^2 fits to the differential spectra EEC^{data}_{parton} and $AEEC^{data}_{parton}$ are performed to obtain these values. The analytic calculations provide good descriptions of the AEEC measurements after the fits, as shown in figure 4 (b), yielding χ^2 values of 14.4, 16.0, 28.8 and 96.0 (16 degrees of freedom) for AB, RSE, KN and FK, respectively. For EEC, the fits deviate somewhat from the measurements for angles below about 60°, as shown in

figure 4 (a), leading to $\chi^2 = 195$, 205, 223 and 340 for AB, RSE, KN and FK (25 degrees of freedom). The FK and KN results have statistical errors which we do not include for the χ^2 determination because these error values are not published. For the Monte Carlo calculations, ERT and GKS, the interpolated point of intersection with the Jetset corrected data value labeled "all" in figure 3 is used to obtain $\Lambda_{\overline{MS}}$.

The statistical errors in table 2 are taken from figure 3. The quoted systematic errors include the uncertainties associated with (i) the measurements, (ii) the extrapolation to the parton level, (iii) the overall normalization and (iv) the sensitivity to the interval of integration. The measurement error is the difference between the value of $\Lambda_{\overline{MS}}$ found from the analysis based on the tracking chambers alone to the one based on the calorimeter alone and has a value of about 90 MeV for EEC and 70 MeV for AEEC. The error in the extrapolation to the parton level is the difference between $\Lambda_{\overline{MS}}$ derived from the Jetset corrected data to that derived from the Herwig corrected data: its typical value is 30 MeV for EEC and and 10 MeV for AEEC. The uncertainty in the overall normalization comes from the 2% deviation from unity, of the parton level corrected EEC distribution integrated over its entire range, which was mentioned in section 3. We conservatively assign an error equal to 4% of the data values in figure 3 to account for this uncertainty, which leads to an error on $\Lambda_{\overline{MS}}$ of about 70 and 50 MeV for EEC and AEEC respectively. The sensitivity to the interval of integration is tested by repeating the analysis using the angular ranges 36.0-144.0°, 43.2-136.8° and 50.4-129.6° for EEC and 22-90°, 29-90° and 36-90° for AEEC and leads to an uncertainty on $\Lambda_{\overline{MS}}$ which is negligible for EEC and about 25 MeV for AEEC. These systematic errors are added in quadrature to give the values in table 2.

For EEC there is a significant difference between the $\Lambda_{\overline{MS}}$ values obtained from the different calculations: these differences are less important for AEEC. We define the theoretical error to be the largest of the differences between the KN and other predictions to obtain

$$\Lambda_{\overline{MS}} = 438 \pm 109\,(\text{exp.})\,^{+150}_{-114}\,(\text{theor.})\ \text{MeV} \quad (\text{EEC}) \tag{6}$$

$$\Lambda_{\overline{MS}} = 211 \pm 92\,(\text{exp.})\,^{+75}_{-20}\,(\text{theor.})\ \text{MeV} \quad (\text{AEEC})$$

or

$$\alpha_s(M^2_{Z^0}) = 0.131 \pm 0.006\,(\text{exp.}) \pm 0.007\,(\text{theor.}) \quad (\text{EEC}) \tag{7}$$

$$\alpha_s(M^2_{Z^0}) = 0.117\,^{+0.007}_{-0.009}\,(\text{exp.})\,^{+0.006}_{-0.002}\,(\text{theor.}) \quad (\text{AEEC})$$

as our measured values for $\Lambda_{\overline{MS}}$ and $\alpha_s(M^2_{Z^0})$, assuming the renormalization scale $\mu = M_{Z^0}$, where the central value and experimental error are from the fits using the KN calculation, while the theoretical error is explained above. The value of α_s from AEEC is in good agreement with that obtained from jet production rates at $\sqrt{s} = M_{Z^0}$ [9,31]; the larger α_s value from EEC may indicate important higher order corrections for that distribution.

5 Renormalization Scale Dependence

In most previous studies of energy correlations, the renormalization scale μ at which the coupling constant $\alpha_s(\mu^2)$ is evaluated was chosen to be the c.m. energy. The scale μ is not a

physical parameter and theoretical results calculated to all orders should not depend on it. For finite orders, the results can exhibit a scale dependence, however. Recent studies have shown that a more general definition, like

$$\mu^2 = f \cdot s \tag{8}$$

with $f = 0.001 - 0.01$, result in a better description of jet production rates at e^+e^- colliders [9,30]. We next perform an $O(\alpha_s^2)$ adjustment of both μ and $\Lambda_{\overline{MS}}$ to the energy correlation measurements, to test the sensitivity of EEC and AEEC to a scale change.

The sensitivity of EEC and AEEC to the renormalization scale can be studied using the KN formula [5], for which the second-order term $B(\chi)$ in (5) is presented as a function of $f = (\mu^2/s)$. We perform fits to the parton level differential measurements, EEC^{data}_{parton} and $AEEC^{data}_{parton}$, fixing f at a given value and determining the $\Lambda_{\overline{MS}}$ value which minimizes χ^2 for that scale. Figure 5 shows the distributions of $\Lambda_{\overline{MS}}$ and χ^2 which result, as a function of f. These figures demonstrate that the $\Lambda_{\overline{MS}}$ value from EEC is quite sensitive to the choice of scale, while the $\Lambda_{\overline{MS}}$ value from AEEC is almost insensitive to this choice. Equivalent results are obtained if the AB calculation of $B(\chi)$ is used instead of that of KN.

A fit to the parton level differential measurements with both $\Lambda_{\overline{MS}}$ and f as free parameters yields

$$\begin{aligned} f = (\mu^2/s) = 0.027 \pm 0.013 \quad ; \quad \Lambda_{\overline{MS}} = 216 \pm 85 \text{ MeV} \qquad \text{(EEC)} \\ f = (\mu^2/s) > 0.29\ (1\ \sigma) \qquad ; \quad \Lambda_{\overline{MS}} = 211 \pm 94 \text{ MeV} \qquad \text{(AEEC)}, \end{aligned} \tag{9}$$

where the errors for $\Lambda_{\overline{MS}}$ include the statistical and experimental systematic uncertainties evaluated as explained in section 4, while those for f are statistical only. We do not quote an "optimal" value for f from AEEC because of the small sensitivity to a scale change for this distribution. Instead we give the value of f at which the χ^2 value is greater by unity than its value at $f = 1$. When evaluated at the Z^0 mass, the $\Lambda_{\overline{MS}}$ values in (9) yield

$$\begin{aligned} \alpha_s(M^2_{Z^0}) = 0.117\,^{+0.006}_{-0.008}\,(\text{exp.}) \quad \text{(EEC)} \\ \alpha_s(M^2_{Z^0}) = 0.117\,^{+0.007}_{-0.009}\,(\text{exp.}) \quad \text{(AEEC)} \end{aligned} \tag{10}$$

or a -12% and 0% difference for EEC and AEEC, respectively, compared to the KN values for α_s obtained at $\mu = \sqrt{s}$ (see table 2 and section 4). This value of α_s from EEC, making use of $\Lambda_{\overline{MS}}$ determined at its preferred renormalization scale, is in good agreement with the α_s value from AEEC.

The question of renormalization scale is also considered by RSE in [3], who predict the values of an angle dependent scale factor $f(\chi)=\mu^2(\chi)/s$. These values, shown in figure 3.2 of [3], lie between 0.001 and 0.015 in the relevant angular regions and so have about the same magnitude as the scale determined from measured jet rates [9]. A fit of $\Lambda_{\overline{MS}}$ to the parton corrected EEC distribution, using this angle dependent scale factor, yields $\Lambda_{\overline{MS}} = 319 \pm 110$ MeV, while for AEEC the result is $\Lambda_{\overline{MS}} = 310 \pm 115$ MeV. The errors include the statistical and systematic uncertainties from the experiment which were considered previously. These $\Lambda_{\overline{MS}}$ values yield in turn $\alpha_s(M^2_{Z^0}) = 0.125^{+0.007}_{-0.009}$ (exp.) for EEC and $\alpha_s(M^2_{Z^0}) = 0.124^{+0.006}_{-0.007}$ (exp.) for AEEC, which differ by about -9% and +2%, respectively, from the RSE values presented in table 2. Thus again, the α_s value from EEC comes into good agreement with that from AEEC, while this latter stays essentially constant, when a small renormalization scale is introduced.

6 Summary and Conclusions

The energy-energy correlation function (EEC) and its asymmetry (AEEC), corrected for initial-state photon radiation and for detector acceptance and resolution, have been measured at $\sqrt{s} = 91$ GeV by the OPAL experiment at LEP. After unfolding the EEC and AEEC distributions for fragmentation, in addition to initial-state radiation and detector effects, the measurements are compared directly to theoretical calculations valid to $O(\alpha_s^2)$, to extract values for the QCD coupling constant α_s. Because the measurements are corrected for fragmentation before being compared to theory, we obtain a clear separation between hadronization and higher order perturbative effects leading to a clean test of the $O(\alpha_s^2)$ predictions.

We obtain values $\alpha_s(M_{Z^0}^2) = 0.131 \pm 0.006\,(\text{exp.}) \pm 0.007\,(\text{theor.})$ and $\alpha_s(M_{Z^0}^2) = 0.117\,^{+0.007}_{-0.009}$ (exp.) $^{+0.006}_{-0.002}$ (theor.) for EEC and AEEC, respectively, assuming the QCD renormalization scale $\mu = M_{Z^0}$. The theoretical error is given by the difference which results from using different calculations. The α_s value from AEEC is in good agreement with values derived from jet multiplicity measurements at the Z^0 peak [9,31].

We have also examined the sensitivity of the energy correlation distributions to changes in the renormalization scale. A simultaneous adjustment of $\Lambda_{\overline{MS}}$ and the scale μ demonstrates that EEC is best fit for $\mu^2/s = 0.027$ and $\Lambda_{\overline{MS}} = 216$ MeV while $\Lambda_{\overline{MS}}$ from AEEC is essentially insensitive to a scale change. An evaluation of $\alpha_s(M_{Z^0}^2)$ for EEC, using the value $\Lambda_{\overline{MS}} = 216$ MeV found at its preferred renormalization scale, yields $\alpha_s(M_{Z^0}^2) = 0.117^{+0.006}_{-0.008}\,(\text{exp.})$, in agreement with the α_s value from AEEC and the jet rates. The larger value of α_s from EEC at $\mu = \sqrt{s}$ is possibly indicative of important higher order corrections for that distribution.

7 Acknowledgments

We thank G. Bélanger, F. Boudjema, P. Nason and G. Kramer for useful discussions or correspondence.

It is a pleasure to thank the SL Division for the efficient operation of the LEP accelerator and their continuing close cooperation with our experimental group. In addition to the support staff at our own institutions we are pleased to acknowledge the following:

Department of Energy, USA
National Science Foundation, USA
Science and Engineering Research Council, UK
Natural Sciences and Engineering Research Council,Canada
Israeli Ministry of Science
Minerva Gesellschaft
The Japanese Ministry of Education, Science and Culture (the Monbusho) and a grant under the Monbusho International Science Research Program.
American Israeli Bi-national Science Foundation.

Direction des Sciences de la Matière du Commissariat à l'Energie Atomique, France
The Bundesministerium für Forschung und Technologie, FRG
and The A.P. Sloan Foundation.

References

[1] C.L. Basham *et al.*, Phys. Rev. Lett. **41** (1978) 1585; Phys.Rev. **D17** (1978) 2298.

[2] A. Ali and F. Barreiro, Phys. Lett. **118B** (1982) 155; Nucl.Phys. **B236** (1984) 269.

[3] D.G. Richards, W.J. Stirling and S.D. Ellis, Phys.Lett. **119B** (1982) 193;
Nucl.Phys. **B229** (1983) 317.

[4] N.K. Falck and G. Kramer, Z.Phys. **C42** (1989) 459.

[5] Z. Kunszt *et al.*, Z Physics at LEP 1, Vol. 1, CERN-89-08, eds. G. Altarelli, R. Kleiss and G. Verzegnassi, Geneva 1989.

[6] R.K. Ellis, D.A. Ross and A.E. Terrano, Nucl.Phys.**B178** (1981) 421.

[7] F. Gutbrod, G. Kramer and G. Schierholz, Z.Phys. **C21** (1984) 235.

[8] T. Sjöstrand, Comp.Phys.Comm. **39** (1986) 347;
T. Sjöstrand and M. Bengtsson, Comp.Phys.Comm. **43** (1987) 367, Jetset version 7.2.

[9] OPAL Collaboration, M.Z. Akrawy *et al.*, Phys.Lett. **B235** (1990) 389.

[10] MARK2 Collaboration, D. Schlatter *et al.*, Phys.Rev.Lett. **49** (1982) 521.

[11] PLUTO Collaboration, Ch. Berger *et al.*, Z.Phys. **C12** (1982) 297.

[12] CELLO Collaboration, H-J. Behrend *et al.*, Z.Phys. **C14** (1982) 95.

[13] MARKJ Collaboration, B. Adeva *et al.*, , Phys.Rev.Lett. **50** (1983) 2051.

[14] JADE Collaboration, W. Bartel *et al.*, Z.Phys. **C25** (1984) 231.

[15] CELLO Collaboration, H.J. Behrend *et al.*, Phys.Lett. **138B** (1984) 311.

[16] TASSO Collaboration, M. Althoff *et al.*, Z.Phys. **C26** (1984) 157.

[17] MAC Collaboration, E. Fernandez *et al.*, Phys.Rev. **D31** (1985) 2724.

[18] MARKJ Collaboration, B. Adeva *et al.*, Phys.Rev.Lett. **54** (1985) 1750.

[19] TASSO Collaboration, W. Braunschweig *et al.*, Z.Phys. **C36** (1987) 349.

[20] MARK2 Collaboration, D.R. Wood *et al.*, Phys.Rev. **D37** (1988) 3091.

[21] TOPAZ Collaboration, I. Adachi *et al.*, Phys.Lett. **B227** (1989) 495.

[22] OPAL Technical Proposal (1983), CERN/LEPC/83-4;
OPAL Collaboration, K. Ahmet *et al.*, The OPAL Detector at LEP, CERN-PPE/90-114, to be submitted to Nucl.Instr. and Meth.

[23] M.Z. Akrawy *et al.*, OPAL Collaboration, Phys. Lett. **B231** (1989) 530;
M.Z. Akrawy *et al.*, OPAL Collaboration, Phys. Lett. **B235** (1990) 379.

[24] OPAL Collaboration, M.Z. Akrawy *et al.*, CERN-EP/90-48, to be published in Z.Phys. **C**.

[25] G. Marchesini and B.R. Webber, Nucl.Phys. **B310** (1988) 461; Herwig version 4.3.

[26] T. Kinoshita *et al.*, J.Math.Phys. **3** (1965) 56;
T.D. Lee and M. Nauenberg, Phys. Rev. **133** (1964) 1549.

[27] T. Sjöstrand *et al.*, Z Physics at LEP 1, Vol. 3, CERN-89-08, eds. G. Altarelli, R. Kleiss and G. Verzegnassi, Geneva 1989.

[28] Review of Particle Properties, Phys. Lett. **204B** (1988) 96.

[29] T.D. Gottshalk and M.P. Shatz, Phys.Lett. **B150** (1985) 451.

[30] G. Kramer and B. Lampe, Z.Phys. **C39** (1988) 101;
N. Magnussen, DESY Report F22-89-01 (1989);
S. Bethke, Z.Phys. **C43** (1989) 331;
AMY Collaboration, I.H. Park *et al.*, KEK-89-53.

[31] MARK2 Collaboration, S. Komamiya *et al.*, Phys.Rev.Lett. **64** (1990) 987;
DELPHI Collaboration P. Abreu et al., CERN-EP/90-89;
L3 Collaboration, B. Adeva et al., L3 Preprint 11.

Bin	χ (deg.)	$EEC(\chi)$ (rad.$^{-1}$)	$EEC(\pi-\chi)$ (rad.$^{-1}$)	$AEEC(\chi)$ (rad.$^{-1}$)
1	0.0-3.6	2.005 ± 0.013 ± 0.283	0.6799 ± 0.0064 ± 0.2331	-1.325 ± 0.014 ± 0.073
2	3.6-7.2	1.250 ± 0.0055 ± 0.0677	1.215 ± 0.0070 ± 0.1908	-0.0349 ± 0.0089 ± 0.1247
3	7.2-10.8	0.9044 ± 0.0035 ± 0.0221	1.090 ± 0.0054 ± 0.0423	0.1855 ± 0.0065 ± 0.0625
4	10.8-14.4	0.6440 ± 0.0026 ± 0.0611	0.8682 ± 0.0042 ± 0.0295	0.2242 ± 0.0049 ± 0.0319
5	14.4-18.0	0.4652 ± 0.0019 ± 0.0551	0.6610 ± 0.0032 ± 0.0465	0.1959 ± 0.0037 ± 0.0105
6	18.0-21.6	0.3473 ± 0.0015 ± 0.0513	0.5168 ± 0.0026 ± 0.0413	0.1695 ± 0.0030 ± 0.0100
7	21.6-25.2	0.2675 ± 0.0012 ± 0.0128	0.4091 ± 0.0021 ± 0.0362	0.1419 ± 0.0024 ± 0.0066
8	25.2-28.8	0.2175 ± 0.0010 ± 0.0327	0.3366 ± 0.0018 ± 0.0361	0.1191 ± 0.0021 ± 0.0043
9	28.8-32.4	0.1835 ± 0.0009 ± 0.0237	0.2787 ± 0.0016 ± 0.0257	0.0952 ± 0.0018 ± 0.0048
10	32.4-36.0	0.1572 ± 0.0008 ± 0.0176	0.2349 ± 0.0014 ± 0.0229	0.0777 ± 0.0016 ± 0.0053
11	36.0-39.6	0.1404 ± 0.0007 ± 0.0172	0.2025 ± 0.0012 ± 0.0163	0.0621 ± 0.0014 ± 0.0035
12	39.6-43.2	0.1262 ± 0.0007 ± 0.0132	0.1789 ± 0.0011 ± 0.0138	0.0527 ± 0.0013 ± 0.0018
13	43.2-46.8	0.1150 ± 0.0007 ± 0.0106	0.1578 ± 0.0010 ± 0.0106	0.0428 ± 0.0012 ± 0.0010
14	46.8-50.4	0.1078 ± 0.0006 ± 0.0071	0.1421 ± 0.0009 ± 0.0083	0.0346 ± 0.0011 ± 0.0009
15	50.4-54.0	0.1000 ± 0.0006 ± 0.0067	0.1285 ± 0.0009 ± 0.0072	0.0284 ± 0.0010 ± 0.0007
16	54.0-57.6	0.0942 ± 0.0006 ± 0.0070	0.1185 ± 0.0008 ± 0.0074	0.0243 ± 0.0010 ± 0.0007
17	57.6-61.2	0.0889 ± 0.0006 ± 0.0038	0.1093 ± 0.0008 ± 0.0071	0.0204 ± 0.0009 ± 0.0036
18	61.2-64.8	0.0861 ± 0.0006 ± 0.0038	0.1027 ± 0.0007 ± 0.0066	0.0166 ± 0.0009 ± 0.0028
19	64.8-68.4	0.0834 ± 0.0005 ± 0.0040	0.0960 ± 0.0007 ± 0.0048	0.0126 ± 0.0009 ± 0.0010
20	68.4-72.0	0.0803 ± 0.0005 ± 0.0028	0.0908 ± 0.0006 ± 0.0047	0.0105 ± 0.0008 ± 0.0027
21	72.0-75.6	0.0790 ± 0.0005 ± 0.0015	0.0873 ± 0.0006 ± 0.0041	0.0083 ± 0.0008 ± 0.0032
22	75.6-79.2	0.0778 ± 0.0005 ± 0.0024	0.0836 ± 0.0006 ± 0.0027	0.0058 ± 0.0008 ± 0.0019
23	79.2-82.8	0.0774 ± 0.0005 ± 0.0029	0.0813 ± 0.0006 ± 0.0033	0.0039 ± 0.0008 ± 0.0009
24	82.8-86.4	0.0771 ± 0.0005 ± 0.0019	0.0791 ± 0.0006 ± 0.0004	0.0020 ± 0.0008 ± 0.0023
25	86.4-90.0	0.0765 ± 0.0005 ± 0.0011	0.0781 ± 0.0006 ± 0.0024	0.0018 ± 0.0008 ± 0.0016

Table 1: The EEC and AEEC distributions at 91 GeV, at the hadron level, unfolded for initial-state radiation and for detector acceptance and resolution. The first error is statistical and includes the statistical uncertainty for the correction factor, the second is systematic. The systematic errors between the different bins are correlated.

	EEC	AEEC
AB [2]	$484 \pm 10 \pm 117$ $(0.133 \pm 0.0005 \pm 0.006)$	$248 \pm 16 \pm 105$ $(0.120 \pm 0.001^{+0.007}_{-0.009})$
RSE [3]	$588 \pm 12 \pm 142$ $(0.138 \pm 0.0006 \pm 0.006)$	$286 \pm 18 \pm 114$ $(0.122 \pm 0.001^{+0.007}_{-0.009})$
KN [5]	$438 \pm 9 \pm 109$ $(0.131 \pm 0.0005 \pm 0.006)$	$211 \pm 13 \pm 91$ $(0.117 \pm 0.001^{+0.007}_{-0.009})$
FK [4]	$324 \pm 7 \pm 84$ $(0.125 \pm 0.0004 \pm 0.006)$	$191 \pm 12 \pm 83$ $(0.115 \pm 0.001^{+0.007}_{-0.009})$
ERT [6]	$335 \pm 7 \pm 83$ $(0.126 \pm 0.0004 \pm 0.005)$	$215 \pm 14 \pm 96$ $(0.117 \pm 0.001^{+0.007}_{-0.010})$
GKS [7]	$480 \pm 10 \pm 117$ $(0.133 \pm 0.0005 \pm 0.006)$	$220 \pm 15 \pm 99$ $(0.118 \pm 0.001^{+0.007}_{-0.010})$

Table 2: $\Lambda_{\overline{MS}}$ in MeV (and $\alpha_s(M_{Z^0}^2)$) obtained from the parton-level EEC and AEEC distributions. The first error is statistical, the second is systematic.

Figure Captions

Figure 1: The measured (a) EEC and (b) AEEC distributions at 91 GeV, at the hadron level, unfolded for detector acceptance and resolution and for initial-state photon radiation. The errors on the data points include the statistical and systematic errors. Also shown are the predictions of the Jetset and Herwig shower Monte Carlos. The inset above (a) shows the correction constants used for the unfolding.

Figure 2: The measured (a) EEC and (b) AEEC distributions at 91 GeV, unfolded to the parton level using either Jetset or Herwig, in comparison to the measured hadron level distributions. The errors are statistical only.

Figure 3: Integrated values of the parton level measurements for (a) EEC and (b) AEEC, unfolded using Jetset corrections, Herwig corrections, Jetset corrections with charged track measurements only or with calorimeter measurements only. Also shown are the theoretical predictions for different values of $\Lambda_{\overline{MS}}$.

Figure 4: Results of the fits of the analytic formulae to the measured (a) EEC and (b) AEEC distributions. The data have been unfolded to the parton level using Jetset, with both charged track and calorimeter information for this illustration.

Figure 5: The best fit values of (a) $\Lambda_{\overline{MS}}$ (in GeV) and (b) the resulting χ^2 per degree-of-freedom, found in an adjustment of $\Lambda_{\overline{MS}}$ to the parton level EEC and AEEC distributions for different choices of the renormalization scale parameter $f = (\mu^2/s)$.

Figure 1

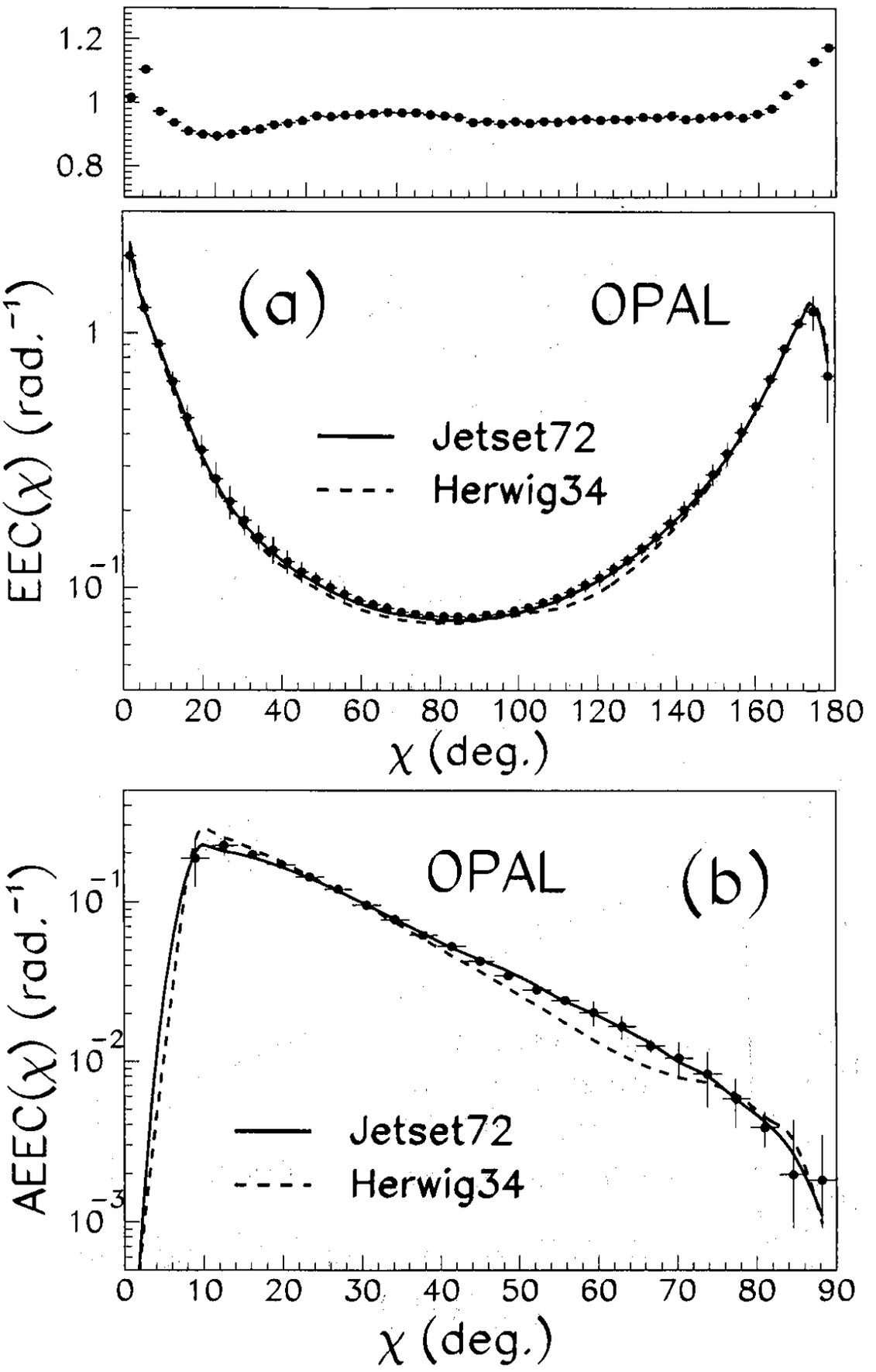
1.2
1
0.8
(a)
OPAL
EEC(χ) (rad.$^{-1}$)
Jetset72
Herwig34
χ (deg.)
OPAL
(b)
AEEC(χ) (rad.$^{-1}$)
Jetset72
Herwig34
χ (deg.)

Figure 2

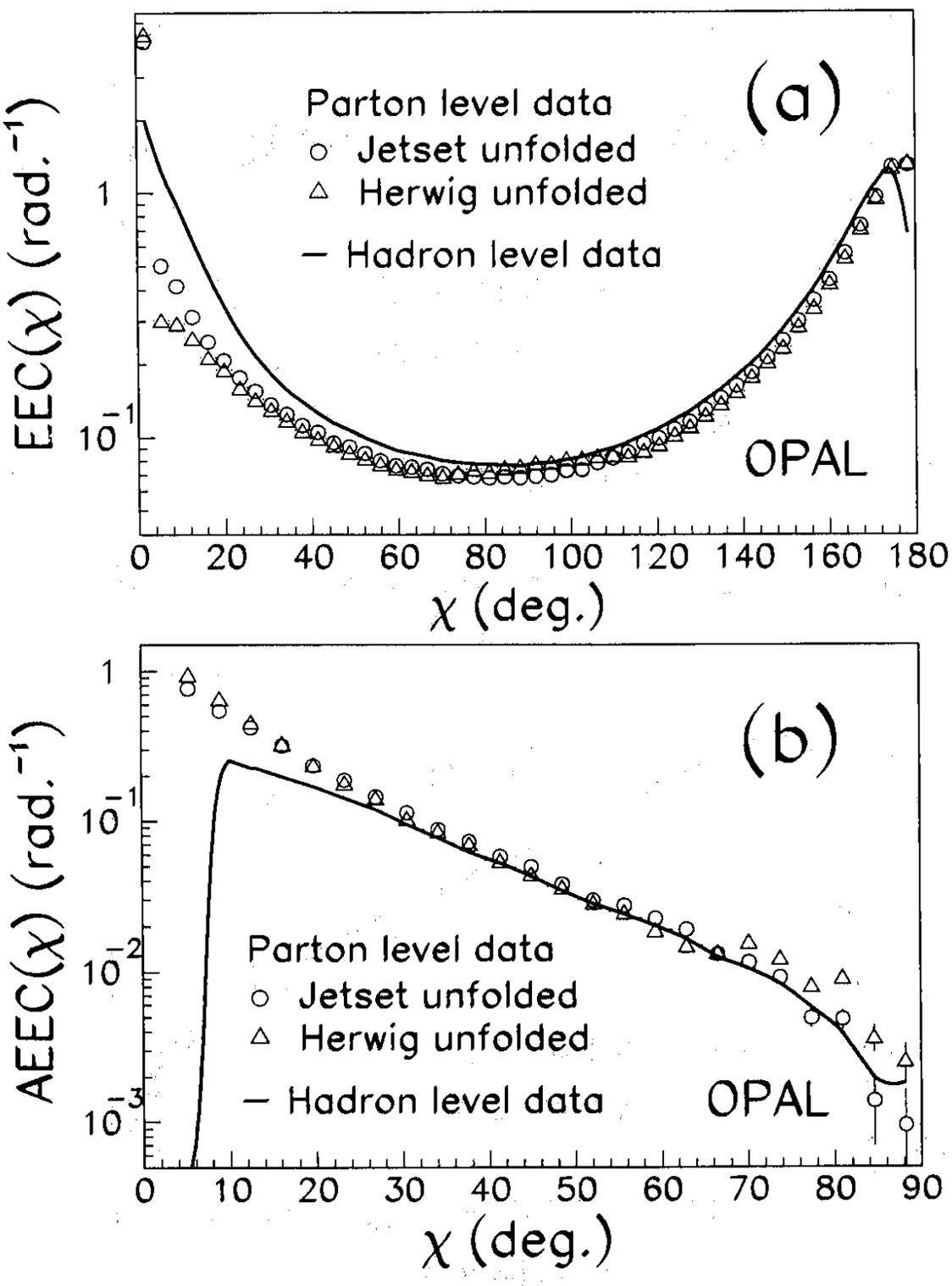
(a)
Parton level data
Jetset unfolded
Herwig unfolded
Hadron level data
OPAL
EEC(χ) (rad.$^{-1}$)
χ (deg.)
(b)
Parton level data
Jetset unfolded
Herwig unfolded
Hadron level data
OPAL
AEEC(χ) (rad.$^{-1}$)
χ (deg.)

Figure 3

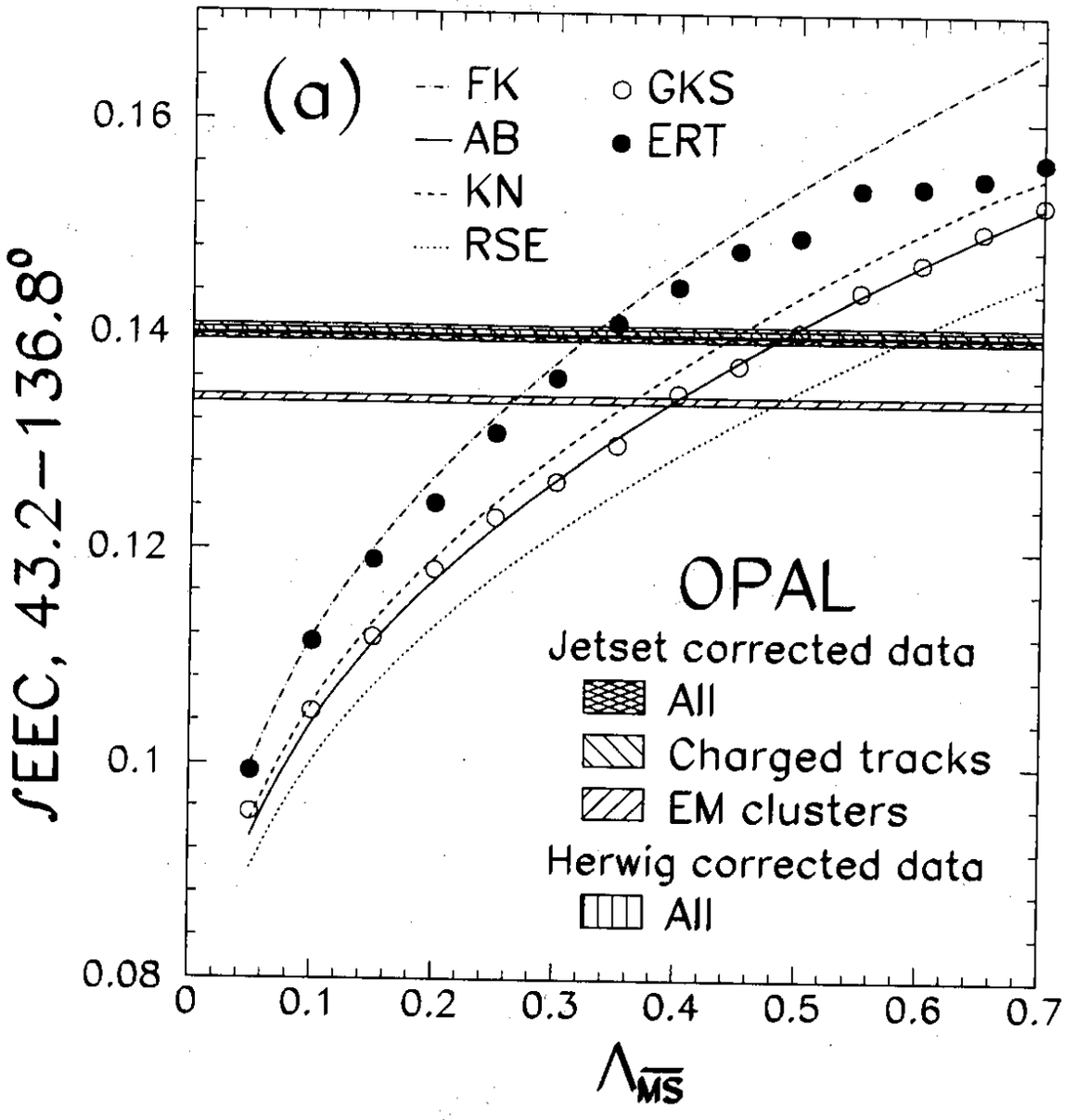
(a)
FK
AB
KN
RSE
GKS
ERT
OPAL
Jetset corrected data
All
Charged tracks
EM clusters
Herwig corrected data
All
∫EEC, 43.2–136.8°
0.16
0.14
0.12
0.1
0.08
0
0.1
0.2
0.3
0.4
0.5
0.6
0.7
Λ MS

Figure 3

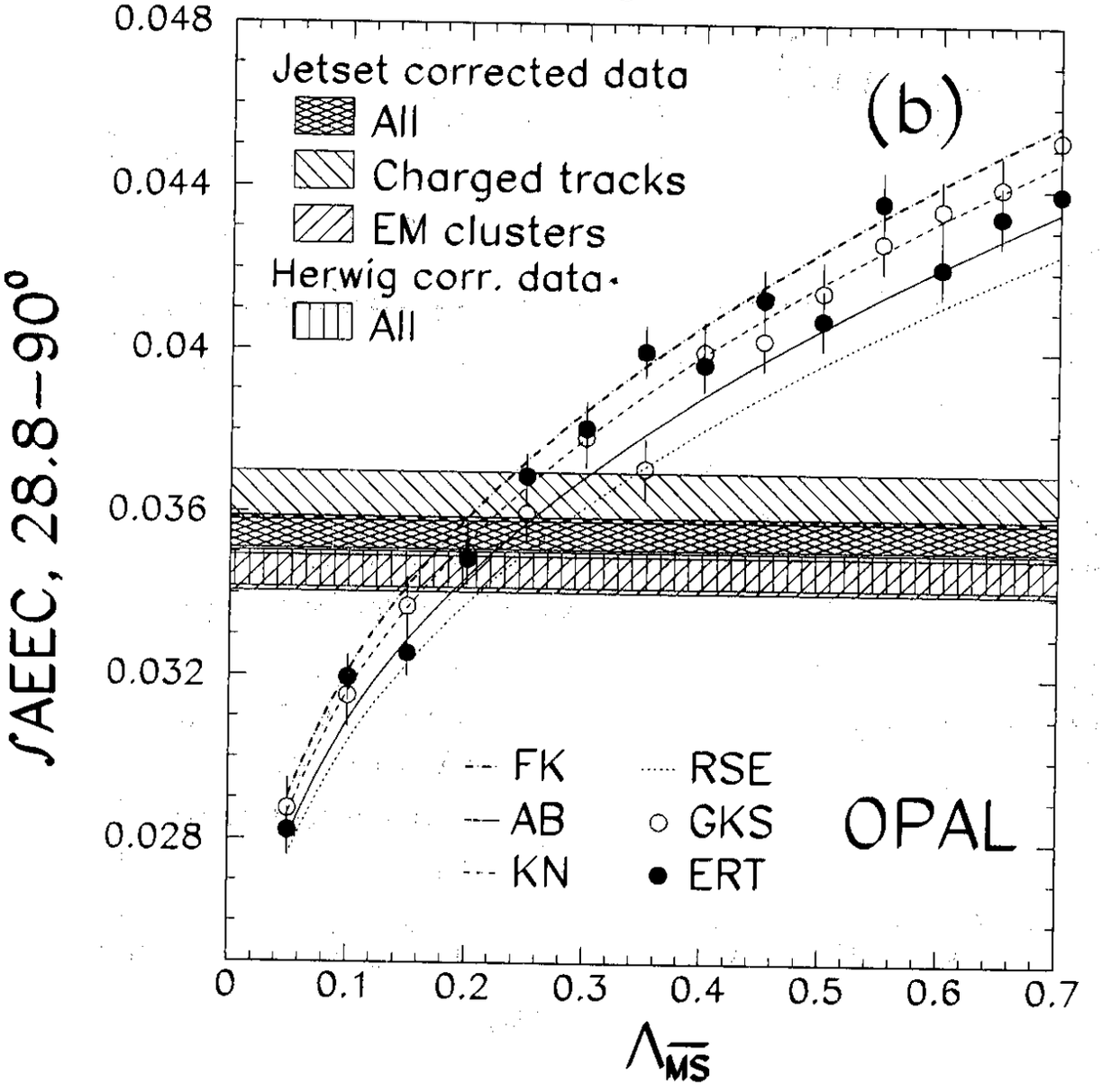
0.048
0.044
0.04
0.036
0.032
0.028
Jetset corrected data
All
Charged tracks
EM clusters
Herwig corr. data
All
(b)
FK
AB
KN
RSE
GKS
ERT
OPAL
0
0.1
0.2
0.3
0.4
0.5
0.6
0.7
$\Lambda_{\overline{MS}}$
$\int$AEEC, 28.8–90°

Figure 4

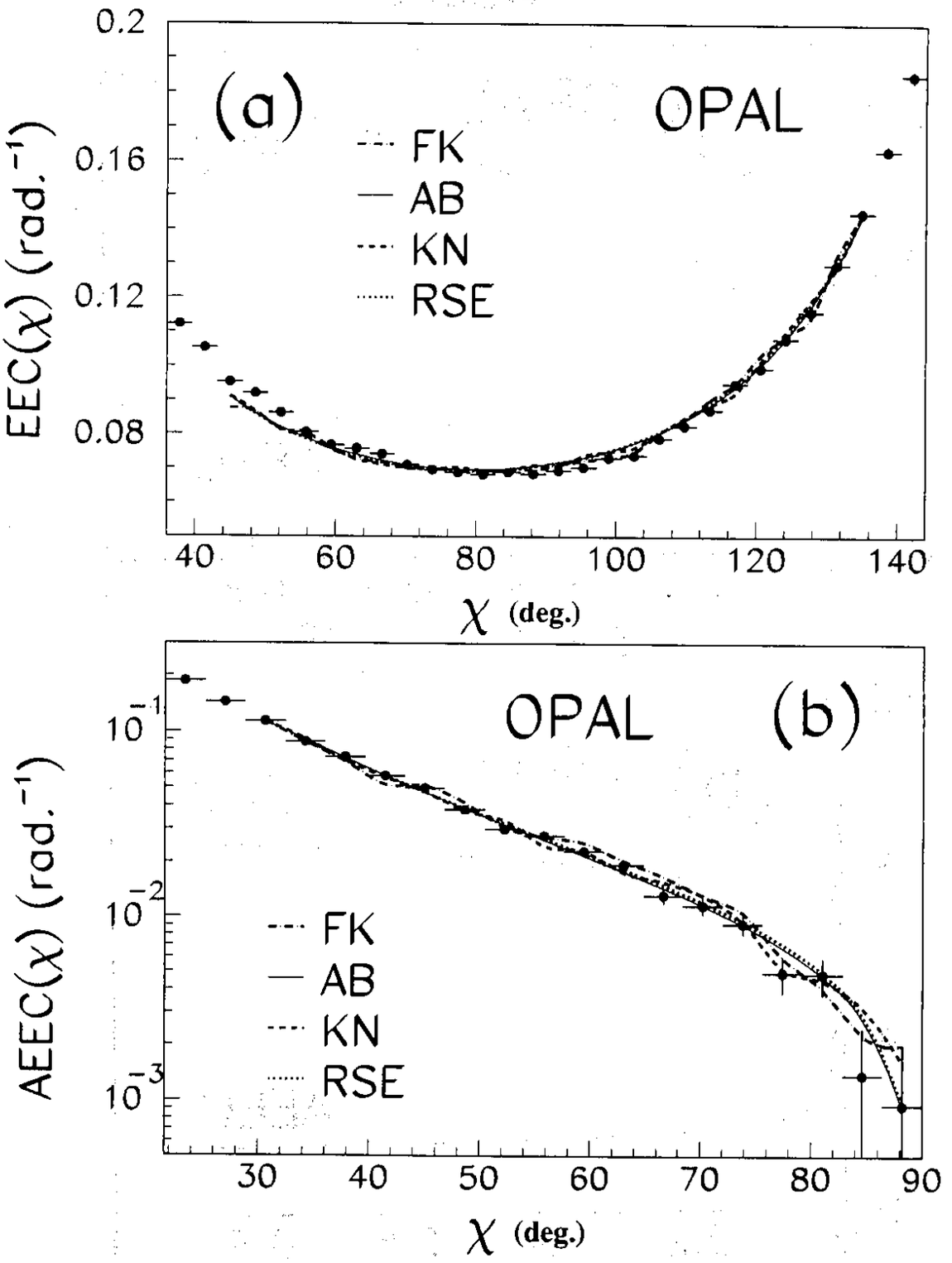
(a)
OPAL
FK
AB
KN
RSE
EEC(χ) (rad.$^{-1}$)
0.2
0.16
0.12
0.08
40
60
80
100
120
140
χ (deg.)
OPAL
(b)
AEEC(χ) (rad.$^{-1}$)
10^{-1}
10^{-2}
10^{-3}
FK
AB
KN
RSE
30
40
50
60
70
80
90
χ (deg.)

Figure 5

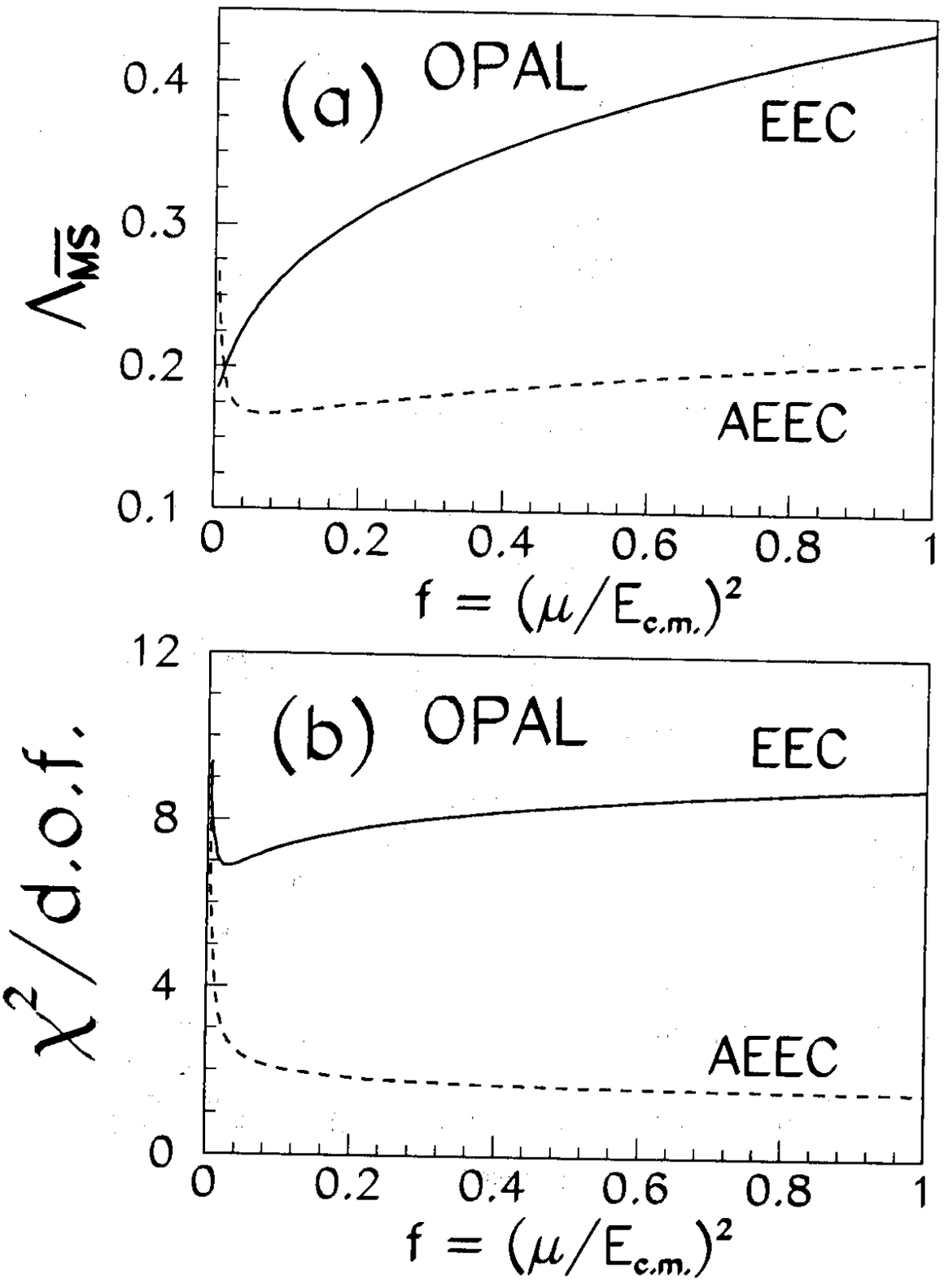

Imprimé au CERN. Prix : 0.70 Fr.